WIRE-BASED TRACKING USING MUTUAL INFORMATION

Juan Andrade-Cetto
Computer Vision Center, UAB
Edifici O, Campus UAB, 08193 Bellaterra, Spain
cetto@cvc.uab.es

Federico Thomas
Institut de Robòtica i Informàtica Industrial, CSIC-UPC
Llorens Artigas 4-6, 08028 Barcelona, Spain
fthomas@iri.upc.edu

Abstract Wire-based tracking devices are an affordable alternative to costly tracking devices. They consist of a fixed base and a platform, attached to the moving object, connected by six wires whose tension is maintained along the tracked trajectory. One important shortcoming of this kind of devices is that they are forced to operate in reduced workspaces so as to avoid singular configurations. Singularities can be eliminated by adding more wires but this causes more wire interferences, and a higher force exerted on the moving object by the measuring device itself. This paper shows how, by introducing a rotating base, the number of wires can be reduced to three, and singularities can be avoided by using an active sensing strategy. This also permits reducing wire interference problems and the pulling force exerted by the device. The proposed sensing strategy minimizes the uncertainty in the location of the platform. Candidate motions of the rotating base are compared selected automatically based on mutual information scores.

Keywords: Tracking devices, Kalman filter, active sensing, mutual information, parallel manipulators.

1. Introduction

Tracking devices, also called 6-degree-of-freedom (6-DOF) devices, are used for estimating the position and orientation of moving objects. Current tracking devices are based on electromagnetic, acoustic, mechanical, or optical technology. Tracking devices can be classified according to their characteristics, such as accuracy, resolution, cost, measurement range, portability, and calibration requirements. Laser tracking systems exhibit good accuracy, which can be less than $1\mu m$ if the system is well calibrated. Unfortunately, this kind of systems are very expensive, their

calibration procedure is time-consuming, and they are sensitive to the environment. Vision systems can reach an accuracy of $0.1mm$. They are low-cost portable devices but their calibration procedure can be complicated. Wire-based systems can reach an accuracy of $0.1mm$, they are also low cost portable devices but capable of measuring large displacements. Moreover, they exhibit a good compromise among accuracy, measurement range, cost and operability.

Wire-based tracking devices consist of a fixed base and a platform connected by six wires whose tension is maintained, while the platform is moved, by pulleys and spiral springs on the base, where a set of encoders give the length of the wires. They can be modelled as 6-DOF parallel manipulators because wires can be seen as extensible legs connecting the platform and the base by means of spherical and universal joints, respectively.

Dimension deviations due to fabrication tolerances, wire-length uncertainties, or wire slackness, may result in unacceptable performance of a wire-based tracking device. In general, the effects of all systematic errors can be eliminated by calibration. Some techniques for specific errors have already been proposed in the literature. For example, a method for compensating the cable guide outlet shape of wire encoders is detailed in Geng and Haynes, 1994, and a method for compensating the deflections caused by wire self-weights is described in Jeong et al., 1999. In this paper, we will only consider wire-length errors which cannot be compensated because of their random nature.

Another indirect source of error is the force exerted by the measuring device itself. Indeed, all commercial wire encoders are designed to keep a large string tension. This is necessary to ensure that the inertia of the mechanism does not result in a wire going slack during a rapid motion. If a low wire force is used, it would reduce the maximum speed of the object to be tracked without the wires going slack. On the contrary, if a high wire force is used, the trajectory of the object to be tracked could be altered by the measuring device. Hence, a trade-off between accuracy and speed arises.

The minimum number of points on a moving object to be tracked for pose measurements is three. Moreover, the maximum number of wires attached to a point is also three, otherwise the lengths of the wires will not be independent. This leads to only two possible configurations for the attachments on the moving object. The *3-2-1 configuration* was proposed in Geng and Haynes, 1994. The kinematics of this configuration was studied, for example, in Nanua and Waldron, 1990 and Hunt and Primrose, 1993. Its direct kinematics can be solved in closed-form by using three consecutive trilateration operations yielding 8 solutions, as

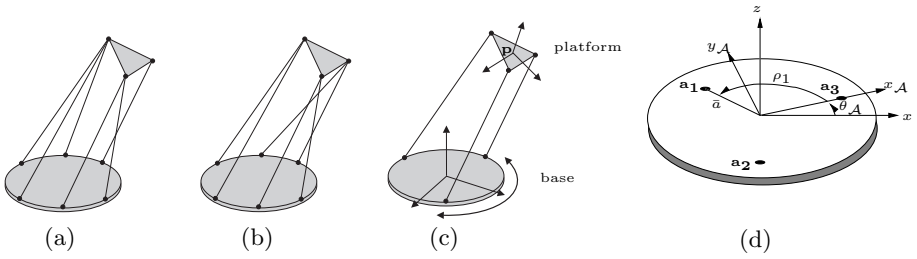

Figure 1. The main two configurations used for wire-based tracking devices: (a) the "3-2-1", (b) the "2-2-2", and (c) the proposed tracking device, with (d) the rotating base

in Thomas et al., 2005. The *2-2-2 configuration* was first proposed in Jeong et al., 1999 for a wire-based tracking device. The kinematics of this configuration was studied, for example, in Griffis and Duffy, 1989, Nanua et al., 1990, and Parenti-Castelli and Innocenti, 1990 where it was shown that its forward kinematics has 16 solutions. In other words, there are up to 16 poses for the moving object compatible with a given set of wire lengths. These configurations can only be obtained by a numerical method. The two configurations above were compared, in terms of their sensitivity to wire-length errors, in Geng and Haynes, 1994. The conclusion was that they have similar properties.

This paper is organized as follows. Section 2 contains the mathematical model of our proposed 3-wire-based sensing device, while Section 3 derives the filtering strategy for tracking its pose. Given that this device has a moving part, Section 4 develops an information theoretic metric for choosing the best actions for controlling it. A strategy to prevent possible wire crossings is contemplated in Section 5. Section 6 is devoted to a set of examples demonstrating the viability of the proposed approach. Finally, concluding remarks are presented in Section 7.

2. Kinematics of the proposed sensor

In order to reduce cable interferences, singularities, and wire tension problems we choose to reduce the number of cables from six to three, and to have the base rotate on its center. Provided the tracked object motion is sufficiently slow, two measurements at different base orientations would be equivalent to a 2-2-2 configuration.

More elegantly, and to let the tracked object move at a faster speed, measurements can be integrated sequentially through a partially observable estimation framework. That is, a Kalman filter.

Consider the 3-wire parallel device in Figure 1(c). It is assumed that the platform configuration is free to move in any direction in $\mathbb{R}^3 \times SO(3)$. Let the pose of our tracking device be defined as the 14-dimensional array

$$\mathbf{x} = \begin{bmatrix} \mathbf{p} \\ \boldsymbol{\theta} \\ \mathbf{v} \\ \boldsymbol{\omega} \\ \theta_{\mathcal{A}} \\ \omega_{\mathcal{A}} \end{bmatrix} , \tag{1}$$

where $\mathbf{p} = (x, y, z)^\top$ is the position of the origin of a coordinate frame fixed to the platform, $\boldsymbol{\theta} = (\psi, \theta, \phi)^\top$ is the orientation of such coordinate frame expressed as yaw, pitch and roll angles, $\mathbf{v} = (v_x, v_y, v_z)^\top$ and $\boldsymbol{\omega} = (\omega_x, \omega_y, \omega_z)^\top$ are the translational and rotational velocities of $\mathbf{p}$, respectively; and $\theta_{\mathcal{A}}$ and $\omega_{\mathcal{A}}$ are the orientation and angular velocity of the rotating base.

Assume that the attaching points on the base $\mathbf{a}_i$, $i = 1, 2, 3$, are distributed on a circle of radius $\bar{a}$ as shown in Figure 1(d). Then, the coordinates of $\mathbf{a}_i$ can be expressed in terms of the platform rotation angle $\theta_{\mathcal{A}}$ as

$$\begin{bmatrix} a_{xi} \\ a_{yi} \\ a_{zi} \end{bmatrix} = \begin{bmatrix} \bar{a}\cos(\rho_i + \theta_{\mathcal{A}}) \\ \bar{a}\sin(\rho_i + \theta_{\mathcal{A}}) \\ 0 \end{bmatrix} . \tag{2}$$

Moreover, let $\mathbf{e}_i$ be the unit norm vector specifying the direction from $\mathbf{a}_i$ to the corresponding attaching point $\mathbf{b}_i$ in the platform; and let l_i be the length of the i-th wire, $i = 1, 2, 3$. The value of $\mathbf{b}_i$ is expressed in platform local coordinates, where $\mathcal{R}$ is the rotation matrix describing the absolute orientation of the platform. Then, the position of the wire attaching points in the platform, in global coordinates, are

$$\mathbf{b}'_i = \mathbf{a}_i + l_i \mathbf{e}_i = \mathbf{p} + \mathcal{R}\mathbf{b}_i . \tag{3}$$

3. State Estimation

We adopt a smooth unconstrained constant-velocity motion model, its pose altered only by zero-mean, normally distributed accelerations and staying the same on average. The Gaussian acceleration assumption means that large impulsive changes of direction are unlikely. In such model the prediction of the position and orientation of the platform at time t plus a time interval τ is given by

$$\begin{bmatrix} \mathbf{p}(t+\tau) \\ \boldsymbol{\theta}(t+\tau) \end{bmatrix} = \begin{bmatrix} \mathbf{p}(t) + \mathbf{v}(t)\tau + \delta\mathbf{a}(t)\tau^2/2 \\ \boldsymbol{\theta}(t) + \boldsymbol{\omega}(t)\tau + \delta\boldsymbol{\alpha}(t)\tau^2/2 \end{bmatrix} , \tag{4}$$

with $\delta\mathbf{a}$ and $\delta\boldsymbol{\alpha}$ zero mean white Gaussian translational and angular acceleration noises. Moreover, the adopted model for the translational and angular velocities of the platform is given by

$$\begin{bmatrix}\mathbf{v}(t+\tau)\\ \boldsymbol{\omega}(t+\tau)\end{bmatrix} = \begin{bmatrix}\mathbf{v}(t)+\delta\mathbf{a}(t)\tau\\ \boldsymbol{\omega}(t)+\delta\boldsymbol{\alpha}(t)\tau\end{bmatrix} . \tag{5}$$

By the same token, the adopted models for the orientation and angular velocity of the base are

$$\begin{bmatrix}\theta_{\mathcal{A}}(t+\tau)\\ \omega_{\mathcal{A}}(t+\tau)\end{bmatrix} = \begin{bmatrix}\theta_{\mathcal{A}}(t)+\omega_{\mathcal{A}}(t)\tau+(\alpha_{\mathcal{A}}(t)+\delta\alpha_{\mathcal{A}}(t))\tau^2/2\\ \omega_{\mathcal{A}}(t)+(\alpha_{\mathcal{A}}(t)+\delta\alpha_{\mathcal{A}}(t))\tau\end{bmatrix} , \tag{6}$$

in which the control signal modifying the base orientation is the acceleration impulse $\alpha_{\mathcal{A}}$.

Since in practice, the measured wire lengths, l_i, $i = 1, 2, 3$, will be corrupted by additive Gaussian noise, δz_i, we have that

$$z_i(t) = l_i(t) + \delta z_i(t) = \|\mathbf{p}(t) + \mathcal{R}(t)\mathbf{b}_i - \mathbf{a}_i(t)\| + \delta z_i(t) . \tag{7}$$

Lastly, the orientation of the moving base is measured by means of an encoder. Its model is simply

$$z_4(t) = \theta_A(t) + \delta z_4(t) . \tag{8}$$

Eqs. 4 and 5 constitute our motion prediction model $\mathbf{f}(\mathbf{x}, \alpha_{\mathcal{A}}, \delta\mathbf{x})$. Eqs. 7 and 8 complete our measurement prediction model $\mathbf{h}(\mathbf{x}, \delta\mathbf{z})$. Now, an Extended Kalman Filter can be used to propagate the platform pose and velocity estimates, as well as the base orientation estimates, and then, to refine these estimates through wire length measurements. To this end, $\delta\mathbf{x} \sim N(\mathbf{0}, \mathbf{Q})$, $\delta\mathbf{z} \sim N(\mathbf{0}, \mathbf{R})$, and our plant Jacobians with respect to the state $\mathbf{F} = \partial\mathbf{f}/\partial\mathbf{x}$, and to the noise $\mathbf{G} = \partial\mathbf{f}/\partial\delta\mathbf{x}$ become

$$\mathbf{F} = \begin{bmatrix}\mathbf{I} & & \tau\mathbf{I} & & & \\ & \mathbf{I} & & \tau\mathbf{I} & & \\ & & \mathbf{I} & & & \\ & & & \mathbf{I} & & \\ & & & & 1 & \tau \\ & & & & & 1\end{bmatrix} \quad \text{and} \quad \mathbf{G} = \begin{bmatrix}\frac{\tau^2\mathbf{I}}{2} & & \\ & \frac{\tau^2\mathbf{I}}{2} & \\ \tau\mathbf{I} & & \\ & \tau\mathbf{I} & \\ & & \frac{\tau^2}{2} \\ & & \tau\end{bmatrix} . \tag{9}$$

The measurement Jacobians $\mathbf{H} = \partial\mathbf{h}/\partial\mathbf{x}$ are simply

$$\mathbf{H}_i(t) = \begin{bmatrix}\mathbf{e}_i(t) & \mathbf{b}_i \times \mathbf{e}_i(t) & \mathbf{0} & \mathbf{0} & \frac{\partial\mathbf{h}_i}{\partial\theta_{\mathcal{A}}} & 0\end{bmatrix} , \tag{10}$$

with

$$\mathbf{e}_i(t) = \frac{\mathbf{p}(t) + \mathcal{R}(t)\mathbf{b}_i - \mathbf{a}_i(t)}{\|\mathbf{p}(t) + \mathcal{R}(t)\mathbf{b}_i - \mathbf{a}_i(t)\|} . \tag{11}$$

Then, by rewriting $\mathcal{R} = \begin{bmatrix} \mathbf{r}_1^\top \\ \mathbf{r}_2^\top \\ \mathbf{r}_3^\top \end{bmatrix}$, the term $\frac{\partial \mathbf{h}_i}{\partial \theta_\mathcal{A}}$ in $\mathbf{H}_i$ becomes

$$\begin{aligned} \frac{\partial \mathbf{h}_i}{\partial \theta_\mathcal{A}} &= 2\bar{a}((x(t) + \mathbf{r}_1(t)^\top \mathbf{b}_i)\sin(\theta_\mathcal{A}(t) + \rho_i) \\ &\quad -(y(t) + \mathbf{r}_2(t)^\top \mathbf{b}_i)\cos(\theta_\mathcal{A}(t) + \rho_i))/l_i(t)\,. \end{aligned} \tag{12}$$

Lastly,

$$\mathbf{H}_4(t) = \begin{bmatrix} \mathbf{0} & \mathbf{0} & \mathbf{0} & \mathbf{0} & 1 & 0 \end{bmatrix}. \tag{13}$$

For the sake of clarity, in the sequel, when needed, time dependencies will be placed as subscripts. Moreover, the term $t + \tau|t$ will be used to indicate an a prior estimate (before measurements are incorporated), and the terms $t|t$ and $t + \tau|t + \tau$ will represent posterior estimates (once measurements are taken into account). The prediction of the state and state covariance are given by

$$\mathbf{x}_{t+\tau|t} = \mathbf{f}(\mathbf{x}_{t|t}, \alpha_\mathcal{A}, \mathbf{0}) \tag{14}$$

$$\mathbf{P}_{t+\tau|t} = \mathbf{F}\mathbf{P}_{t|t}\mathbf{F}^\top + \mathbf{G}\mathbf{Q}\mathbf{G}^\top \tag{15}$$

and, the revision of the state estimate and state covariance are

$$\mathbf{x}_{t+\tau,t+\tau} = \mathbf{x}_{t+\tau|t} + \mathbf{K}(\mathbf{z}_{t+\tau} - \mathbf{h}(\mathbf{x}_{t+\tau|t}, \mathbf{0})) \tag{16}$$

$$\mathbf{P}_{t+\tau|t+\tau} = (\mathbf{I} - \mathbf{K}\mathbf{H})\mathbf{P}_{t+\tau|t} \tag{17}$$

with $\mathbf{I}$ the identity matrix, and $\mathbf{K} = \mathbf{P}_{t+\tau|t}\mathbf{H}^\top(\mathbf{H}\mathbf{P}_{t+\tau|t}\mathbf{H}^\top + \mathbf{R})^{-1}$ the usual Kalman gain.

4. Information Gain

This section builds from basic principles a metric for the expected information gain as a result of performing a given action, and develops from it, a strategy for controlling the base orientation. The aim is to rotate the base in the direction that most reduces the uncertainty in the entire pose state estimate, by using the information that should be *gained* from future wire measurements were such a move be made, but taking into account the information *lost* as a result of moving with uncertainty.

The essential idea is to use mutual information as a measurement of the statistical dependence between two random vectors, that is, the amount of information that one contains about the other. Consider the states $\mathbf{x}$, and the measurements $\mathbf{z}$. The mutual information of the

two continuous probability distributions $p(\mathbf{x})$ and $p(\mathbf{z})$ is defined as the information about $\mathbf{x}$ contained in $\mathbf{z}$, and is given by

$$I(\mathbf{x}, \mathbf{z}) = \int_{\mathbf{x},\mathbf{z}} p(\mathbf{x}, \mathbf{z}) \log \frac{p(\mathbf{x}, \mathbf{z})}{p(\mathbf{x})p(\mathbf{z})} d\mathbf{x} d\mathbf{z} \,. \tag{18}$$

Note how mutual information measures the independence between the two vectors. It equals zero when they are independent, $p(\mathbf{x}, \mathbf{z}) = p(\mathbf{x})p(\mathbf{z})$. Mutual information can also be seen as the relative entropy between the marginal density $p(\mathbf{x})$ and the conditional $p(\mathbf{x}|\mathbf{z})$

$$I(\mathbf{x}, \mathbf{z}) = \int_{\mathbf{x},\mathbf{z}} p(\mathbf{x}, \mathbf{z}) \log \frac{p(\mathbf{x}|\mathbf{z})}{p(\mathbf{x})} d\mathbf{x} d\mathbf{z} \,. \tag{19}$$

Given that our variables of interest can be described by multivariate Gaussian distributions, the parameters of the marginal density $p(\mathbf{x})$ are trivially the Kalman prior mean $\mathbf{x}_{t+\tau|t}$ and covariance $\mathbf{P}_{t+\tau|t}$. Moreover, the parameters of the conditional density $p(\mathbf{x}|\mathbf{z})$ come precisely from the Kalman update equations $\mathbf{x}_{t+\tau|t+\tau}$ and $\mathbf{P}_{t+\tau|t+\tau}$. Substituting the genaral form of the Gaussian distribution in Eq. 19, we can obtain a closed formula

$$I(\mathbf{x}, \mathbf{z}) = \frac{1}{2} \left(\log |\mathbf{P}_{t+\tau|t}| - \log |\mathbf{P}_{t+\tau|t+\tau}| \right) \,. \tag{20}$$

Thus, in choosing a maximally mutually informative motion command, we are maximizing the difference between prior and posterior entropies (MacKay, 1992). In other words, we are choosing the motion command that most reduces the uncertainty of $\mathbf{x}$ due to the knowledge of $\mathbf{z}$.

The real-time requirements of the task preclude using an optimal control strategy to search for the base rotation command that ultimately maximizes our mutual information metric. Instead, we can only evaluate such metric for a discrete set of actions within the range of possible commands, and choose the best action from those. The set of possible actions is a discretization of a range of accelerations.

5. Preventing Wire Crossings

Providing the base with the ability to rotate has the added advantage of increasing the range of motion of the tracked platform; mainly, for rotations along the vertical axis. One of the main difficulties however, is in appropriately choosing base rotation commands so as to prevent wire crossings. Considering that wire end-point displacements are sufficiently small per sampling interval, the trajectory described by each

wire can be assumed to be circumscribed within a tetrahedron. One way to predict wire crossings is by checking whether the tetrahedra described by the current and posterior poses for each wire intersect each other; each tetrahedron described by the four attaching points $\{\mathbf{a}_{i,t|t}, \mathbf{a}_{i,t+\tau|t}, \mathbf{b}'_{i,t|t}, \mathbf{b}'_{i,t+\tau|t}\}$.

A very fast test of tetrahedra intersection is based on the Separating Axis Theorem described in the computer graphics literature (Ganovelli et al., 2003). The test consists on checking whether the plane lying on the face of one tetrahedron separates the two of them. If this is not the case, the test continues to find out if there exists a separating plane containing only one edge on one of the tetrahedra.

6. Implementation and Examples

6.1 Mechanical Considerations

In a cable extension transducer, commonly known as a string pot, the tension of the cable is guaranteed by a spring connected to its spool. Using a cable guide, the cable is allowed to move within a 20° cone, making it suitable for 3D motion applications. There are cable guides that permit 360° by 317° displacement cable orientation flexibility. Manufacturers of such sensors are Celesco Transducer Products Inc., SpaceAge Control Inc., Carlen Controls Inc., and several others.

String pots provide a long range $(0.04 - 40m)$, with typical accuracy of 0.02% of full scale. The maximum allowable cable velocity is about $7.2m/s$ and the maximum cable acceleration is about $200m/s^2$.

The usefulness of a tracking device depends on whether it can track the motion fast enough. This ability is determined by the lag, or latency, between the change of the position and orientation of the target being tracked and the report of the change to the computer. In virtual reality applications, lags above 50 milliseconds are perceptible to the user. In general, the lag for mechanical trackers is typically less than $5ms$.

6.2 Maximum Base Rotation Speed

The quality of the estimated pose is directly influenced by the velocity at which the base can rotate. To determine the range of motion velocities that can be tracked with our system, a tracking simulation was repeated limiting the base rotation velocity. A set of 20 runs was conducted, varying the maximum platform rotation speed from 0 to 1 rad/s, and with time steps of 0.01 s; the tracked object translating at a constant velocity of 0.2 m/s along the x axis, and rotating at $\frac{\pi}{10} rad/s$ about an axis perpendicular to the base. Fig. 2 shows the average error of the pose

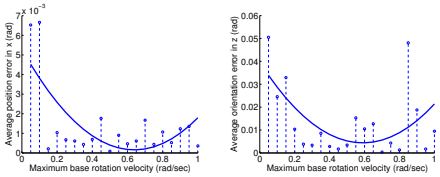

Figure 2. Average position and orientation recovery error as a function of the maximum platform rotation speed, and 2nd order curve fit.

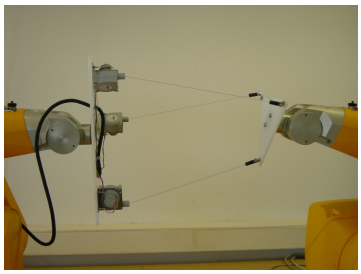

Figure 3. Wire sensing device. The rotating base is attached to the Staubli arm shown in the left side. The moving platform is attached to the arm shown to the right.

estimation as a function of the maximum base rotational velocity. The best pose estimations are achieved when the base rotates at twice the speed of the tracked object, approximately $\frac{\pi}{5} rad/s$ for this experiment.

6.3 Pure rotations

A second experiment consisted in testing the tracking system under pure rotations along the vertical axis. The idea is to show that, whenever cable crossing allows it, the largest acceleration commands are selected. This is because prior and posterior entropy difference is maximized for largest possible configuration changes. The attaching points in both the base and the platform have been arranged to form equilateral triangles. Their coordinates can be found in Tb. 1, and refer to the frames shown in Figure 1. The actual testbench used is shown in Figure 6.3.

For this example, the object to be tracked rotated at $\frac{\pi}{10}$ rad/s, whilst kept at a distance of 1 m from the base. The maximum base rotation speed was limited to $\frac{\pi}{5}$ rad/s, and the limit for possible base acceleration command was set to 5 rad/sec^2. Figure 4(a) shows the evolution of the wire length measurements along the trajectory. Wire length sensors are modeled with additive Gaussian noise with zero mean and 1 mm standard deviation. Moreover, readings of the base orientation are also

Table 1. Coordinates of the attaching points (in meters) in their local coordinate frames.

	x	y	z		x	y	z
$\mathbf{a}_1$	0.3000,	0.0000,	0.0000	$\mathbf{b}_1$	0.1000,	0.0000,	0.0000
$\mathbf{a}_2$	-0.1500,	0.2598,	0.0000	$\mathbf{b}_2$	-0.0500,	0.0866,	0.0000
$\mathbf{a}_3$	-0.1500,	-0.2598,	0.0000	$\mathbf{b}_3$	-0.0500,	-0.0866,	0.0000

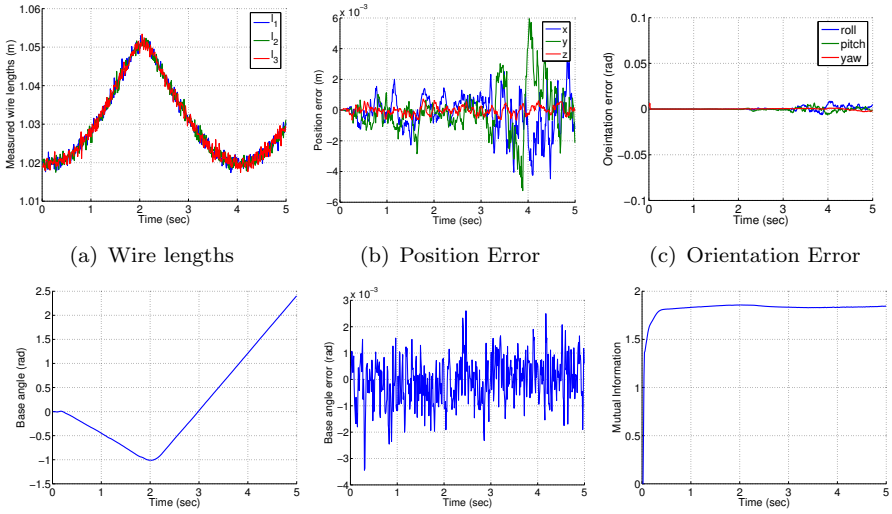

(a) Wire lengths (b) Position Error (c) Orientation Error

(d) Base angle (e) Base angle error (f) Mutual Info.

Figure 4. Wire tracking of pure rotations along an axis perpendicular to the base platform.

modeled with zero mean white additive Gaussian noise with 0.001 rad standard deviation. Figures 4(b) and 4(c) show the tracked object position and orientation recovery errors, respectively. The motion of the rotating base is depicted in Figures 4(d)-4(e), showing that commands for maximal platform rotation velocities are being selected from our mutual information metric (Figure 4(f)).

6.4 Compound motions

In this last example, the tracked object moves back and forth in the three Cartesian components along a line from $(1, 1, 1)$ to $(2, 2, 2)$ meters, whilst rotating $\pi/3rad$ about its center in all raw, pitch and yaw com-

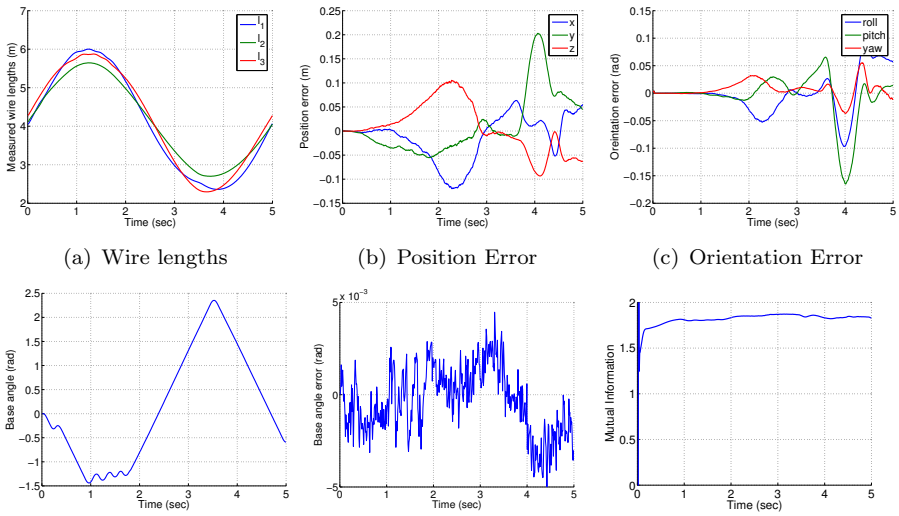

(a) Wire lengths (b) Position Error (c) Orientation Error

(d) Base angle (e) Base angle error (f) Mutual Info.

Figure 5. Wire tracking of compound motion.

ponents. This experiment shows that for compound motions it is more difficult to disambiguate orientation error, while still doing a good job at tracking the correct object pose. Once more, the maximum base rotation speed was limited to $\frac{\pi}{5}$ rad/sec, and the limit for possible base acceleration command was set to 30 rad/sec^2. Figure 5(a) shows the evolution of wire length measurements for this example. The tracked object position and orientation errors is shown in Figures 5(b) and 5(c). The motion of the rotating base is depicted in Figures 5(d)-5(e). And, our mutual information action selection mechanism is shown in Figure 5(f).

7. Conclusion

An active sensing strategy for a wire tracking device has been presented. It has been shown how by allowing the sensor platform rotate about its center, a wider range of motions can be tracked by reducing the number of wires needed from 6 to 3. Moreover, platform rotation is performed so as to maximize the mutual information between poses and measurements, and at the same time, so as to prevent wire wrappings as far as possible.

Acknowledgments

J. Andrade-Cetto completed this work as a Juan de la Cierva Postdoctoral Fellow of the Spanish Ministry of Education and Science under project TIC2003-09291 and was also supported in part by projects DPI 2004-05414, and the EU PACO-PLUS project FP6-2004-IST-4-27657. F. Thomas was partially supported by the Spanish Ministry of Education and Science, project TIC2003-03396, and the Catalan Research Commission, through the Robotics and Control Group.

References

Bruynickx, H. (1999). Forward kinematics for hunt-primrose parallel manipulators. *Mechanism and Machine Theory*, 34:657–664.

Davison, A. (2005). Active search for real-time vision. In *Proceedings of the IEEE International Conference on Computer Vision*, pages 66–73, Beijing.

Ganovelli, F., Ponchio, F., and Rocchini, C. (2003). Fast tetrahedron-tetrahedron overlap algorithm. *ACM Journal of Graphics Tools*, 7(4).

Geng, Z. J. and Haynes, L. S. (1994). A 3-2-1 kinematic configuration of a Stewart platform and its application to six degree of freedom pose measurements. *Robotics and Computer-Integrated Manufacturing*, 11(1):23–34.

Griffis, M. and Duffy, J. (1989). A forward displacement analysis of a class of Stewart platforms. *Journal of Robotic Systems*, 6(6):703–720.

Hunt, K. and Primrose, E. (1993). Assembly configurations of some in-parallel-actuated manipulators. *Mechanism and Machine Theory*, 28(1):31–42.

Jeong, J., Kim, S., , and Kwak, Y. (1999). Kinematics and workspace analysis of a parallel wire mechanism for measuring a robot pose. *Mechanism and Machine Theory*, 34(6):825–841.

MacKay, D. J. C. (1992). Information based objective functions for active data selection. *Neural Computation*, 4(4):589–603.

Merlet, J. P. (2006). *Parallel Robots*, volume 128 of *Solid Mechanics and its Applications*. Springer, New York, 2nd edition.

Nanua, P. and Waldron, K. (1990). Direct kinematics solution of a special parallel robot structure. In *Proceedings of the 8th CISM-IFToMM Symposium on Theory and Practice of Robots and Manipulators*, pages 134–142, Warsaw.

Nanua, P., Waldron, K., and Murthy, V. (1990). Direct kinematic solution of a Stewart platform. *IEEE Transactions on Robotics and Automation*, 6(4):438–444.

Parenti-Castelli, V. and Innocenti, C. (1990). Direct displacement analysis for some classes of spatial parallel machanisms. In *Proceedings of the 8th CISM-IFToMM Symposium on Theory and Practice of Robots and Manipulators*, pages 126–133, Warsaw.

Thomas, F., Ottaviano, E., Ros, L., and Ceccarelli, M. (2005). Performance analysis of a 3-2-1 pose estimation device. *IEEE Transactions on Robotics*, 21(3):288–297.

Vidal-Calleja, T., Davison, A., Andrade-Cetto, J., and Murray, D. (2006). Active control for single camera SLAM. In *Proceedings of the IEEE International Conference on Robotics and Automation*, Orlando. To appear.